2017-11

An integrated approach for the installation of a wave farm

Arean, N

10.1016/j.energy.2017.07.114
Energy

An integrated approach for the installation of a wave farm

N. Arean[1], R. Carballo[1*], G. Iglesias[2]

[1]*Univ. of Santiago de Compostela, Hydraulic Eng., Campus Univ. s/n, 27002 Lugo, Spain*

[2]*Univ. of Plymouth, School of Marine Science and Engineering, Marine Building, Drakes Circus, Plymouth PL4 8AA, United Kingdom*

Abstract

The installation of a wave farm involves the appropriate selection of a location and a wave energy converter (WEC) for harnessing the energy resource. There is typically a considerable number of options both regarding the site and the technology, and choosing the optimum WEC-site combination is not straightforward. An integrated approach is demonstrated in this work by means of a case study in Burela (Galicia, NW Spain)—an area that has been proposed for wave energy exploitation. Three possible locations are defined with a view to avoiding potential environmental impacts and the interference of the wave farm with existing uses of the marine space. The power performance of six technologies at the selected locations is computed by means of a comprehensive methodology based on high-resolution numerical modelling, which guarantees accurate and reliable results. Significant spatial variability of the resource over short length scales is found, which translates into large variations in the performance of the various WECs considered. On this basis, the optimum site and WEC for the area are determined, and the integrated approach—which may be used in any other region of interest—is demonstrated.

*Corresponding author. Tel.: +34-982-285900; fax.: +34-982-285926

E-mail address: rodrigo.carballo@usc.es

Keywords: power performance; high-resolution modelling; ICZM; WEC-site combination.

1. Introduction

The Atlantic European coastline boasts a vast wave energy resource e.g. [1-3]; in particular, the Iberian Peninsula (Spain and Portugal), France, UK, Norway and Ireland have been shown to be of interest for wave energy exploitation e.g.[4]. As regards the Iberian Peninsula, the most energetic region is Galicia (NW Spain), with up to 40-45 kW m^{-1} of annual average wave power [5]—and this is the region where the study area of this work is located.

On the other hand, over recent years a gamut of Wave Energy Converters (WECs) are steadily progressing towards a commercial stage [4,6]. They are based on different principles of operation [7] namely: wave activated bodies [8]; overtopping devices [9] and oscillating water columns [10]. In view of this international interest and investment on R&D, wave farms are likely to be deployed in the coming years. They will be of particular interest in supplying the energy requirements of islands and other peripheral communities, as well as of coastal facilities such as ports e.g. [11-13]. Finally, the selection of the appropriate technology and location for installing a wave farm in a region depends not only on the available resource and the performance that WECs can attain at particular locations [14], but also on socioeconomic and environmental aspects, such as maritime routes, fishing and aquaculture areas, and marine reserves. In this context, over the last years different optimization procedures have been developed and implemented so as to consider part of these aspects in the selection of the most appropriate areas [15], thereby leading to an integrated approach for wave energy exploitation e.g. [16,17].

*Corresponding author. Tel.: +34-982-285900; fax.: +34-982-285926
E-mail address: rodrigo.carballo@usc.es

Despite the interest of previous studies so as to install a wave farm in a region, they are usually focused on the selection of the optimum areas from an economic, environmental and energy availability standpoint, not leading to the selection of the most appropriate technology in terms of performance, which is in turn a key aspect for the viability of a wave farm project. The main objective of this work is to implement a procedure for defining the optimum characteristics of a wave farm in a coastal region taking into account all the relevant aspects affecting the exploitation of the wave resource. The procedure is illustrated through a case study next to the Port of Burela, on the North coast of Galicia (**Figure 1**); this area, of great environmental value and with an important sea-related activity, has been proposed for wave energy exploitation [18].

[FIGURE 1]

For this purpose, three potential sites are selected so as not to represent an environmental impact and interference of the wave farm with other uses of the marine space. Next, a comparative study considering six different types of WECs at the selected sites is carried out. Two main aspects must be considered for estimating the energy production of a WEC at a specific site [19]: (i) the power matrix of the WEC, which provides the efficiency of the device under different sea conditions; (ii) the characterization matrix of the wave resource, which characterizes the resource at the location of interest in terms of the parameters of the sea states that provide the energy. The combination of these two matrices allows the accurate computation of the energy production of a specific WEC at each location of interest, which is the basis for selecting the most appropriate WEC-site combination for the wave farm in terms of energy performance. The power matrix is typically provided by the technology

developers e.g. [6], whereas the resource characterization matrix must be determined following a methodology that ensures sufficient resolution. The methodology followed in this work, developed and successfully applied in previous studies [19-23], involves three main steps [24]: (i) the characterization of the offshore wave resource based on instrumental data; (ii) the selection and propagation of the relevant wave energy cases, representing virtually 100% of the exploitable resource; (iii) the reconstruction of the wave energy resource at the sites of interest in the form of high-resolution characterization matrices. The resulting matrices at the sites of interest are then combined with the power matrix of the devices selected. As a result, a value of average annual energy production is obtained for each WEC-site pair, and the basis for an informed decision is thus provided.

The information made available through the present piece of research combines high-resolution performance results of different WEC at coastal sites selected through an integrated coastal zone management (ICZM) approach. This information, not previously available for the region of interest (Port of Burela and surroundings, N Spain), will lead to the definition of the optimum characteristics of a wave farm in this coastal area, of major interest for wave energy exploitation. This article is structured as follows. In Section 2 the complete procedure for the definition of the locations and technologies of interest for further analysis is presented, along with the implementation of the wave resource characterization and the methodology for computing the energy production. The energy production and performance results are presented and thoroughly discussed in Section 3, and the main conclusions are drawn in Section 4.

2. Definition and implementation of the procedure

2.1. Locations of interest for wave energy exploitation

In addition to the energy available, the socioeconomic and environmental aspects are also of major relevance in selecting the most appropriate sites for installing a wave farm in a region [15,17]. In effect, an integrated coastal zone management approach is required to avoid environmental damage [16] and the interference with other coastal uses [25,26], or in other words, to allow the sustainable development of the coast. In particular, marine reserves (mainly Natura 2000 network), fishing activity in the area, shellfish zones, and maritime routes are factors that should be borne in mind when selecting the areas for energy exploitation. With this in view, a thorough analysis was conducted in this work on the socioeconomic uses and environmental aspects near the Port of Burela which could be affected by wave energy exploitation (**Figure 2**).

[FIGURE 2]

On the basis of the results obtained, three locations were selected (**Figure 3**), not causing interference with existing uses of the marine space along with potential environmental impacts, which are considered for the analysis of the energy production and performance of different wave energy converters of interest.

[FIGURE 3]

2.2. Selected devices

Based on the analysis of current technologies, e.g. [6], six different WECs were selected: Small bottom-referenced Heaving Buoy (Bref-HB), Bottom-fixed Heave-Buoy Array (B-HBA), Bottom-fixed Oscillating Flap (B-OF), Pelamis, Floating Oscillating Water Column (F-OWC) and Archimedes Wave Swing (AWS). These WECs were

selected because they are in an advanced development status. Furthermore, given that their design limits their operation to a specific depth range, they are only considered at the locations allowing their installation (**Table 1**).

[TABLE 1]

The efficiency of a WEC is given by its power matrix, which can be expressed in two forms: (i) as percentages of the total available wave energy, or (ii) as power output values. The efficiency is highly dependent on the wave conditions, which are defined by the significant wave height, H_{m0} [m], and the energy period, T_e [s]. In the present study, the power matrix of the six devices selected is expressed in terms of power output (**Figure 4**). Another key aspect is the resolution of the intervals of the power matrix. This resolution is provided in intervals of spectral wave height, H_{m0}, and energy period, T_e, which in turn varies depending on the technology; at present, the highest resolution available is 0.5 m of H_{m0} and 0.5 s of T_e. It follows that the wave resource characterization matrix at a location of interest should have a resolution of the same level as that of the power matrix of the WEC for which energy production computations are to be conducted.

[FIGURE 4]

2.3. Oceanographic data

The offshore wave data were obtained from the Estaca de Bares buoy located at coordinates 44º 7.524’ N, 7º 41.14’ W at roughly 2000 m water depth providing hourly records of directional sea states over a total period of 17 years. The buoy records are

composed by spectral moments, m_n [m^2Hz^{-n}], characterizing each sea state, which are given by e.g. [27]:

$$m_n = \int_0^{2\pi} \int_0^{\infty} f^n S(f,\theta) df d\theta \quad (1)$$

where f [Hz] is the frequency, S [$m^2Hz^{-1}deg^{-1}$] the spectral energy density and θ [º] the direction of propagation. The minus first, m_{-1}, and zero moments, m_0, are used for obtaining H_{m0}, T_e, and the mean wave direction, θ_m e.g.[27,28] as follows:

$$H_{m0} = 4(m_0)^{1/2} \quad (2)$$

$$T_e = \frac{m_{-1}}{m_0} \quad (3)$$

$$\theta_m = m_0^{-1} \int_0^{2\pi} \int_0^{\infty} \theta S(f,\theta) df d\theta \quad (4)$$

As a result, each sea state record is defined based on the three above parameters as determined by Eqs. (2)-(4). Figure 5 shows the annual wave height and direction distribution at the Estaca de Bares buoy.

[FIGURE 5]

2.4. Wave resource reconstruction

2.4.1. Selection and propagation of deepwater conditions

In the present application, the wave energy resource distribution at the deepwater buoy is transferred towards the shore in order to reconstruct the characterization matrices at the coastal locations of interest. With this aim, the probability of occurrence of each

deepwater sea state is analyzed based on the energy bin concept [24]. Energy bins are defined as joint intervals of H_{m0}, T_e and θ_m of a specific size. In the present application, the size of these intervals is set to 0.5 m and 0.5 s for H_{m0} and T_e, respectively (corresponding to the highest resolution of the power matrices, as indicated) and 22.5º of θ_m. Each energy bin provides the information regarding the occurrence, O_b [h], and energy per meter of wave front, E_b, [Whm^{-1}] supplied by each interval over an average year, which is calculated from the wave power, J [Wm^{-1}], computed according to linear wave theory as [29]:

$$J = \frac{\rho g}{32} H_{m0}^2 \left(1 + \frac{2kd}{\sinh(2kd)} \right) \frac{gT_e}{2\pi} \tanh(kd) \quad (5)$$

where ρ [kgm^{-3}] is the density of seawater, g [ms^{-2}] the acceleration of gravity, k [m^{-1}] the wave number, and d [m] the water depth at the buoy position. Once the occurrence and power are obtained, E_b is computed.

The resulting energy bins can be plotted in a scatter energy diagram representing the distribution of the energy resource, i.e. the characterization matrix. In **Figure 6,** the omnidirectional characterization matrix at the deepwater buoy location is presented.

[FIGURE 6]

Next, the offshore wave climate represented by this resource characterization matrix is transferred towards the coastal locations of interest through high-resolution numerical modelling. In this task, encompassing 100% of the offshore resource would have incurred large computational costs, and a compromise between accuracy and efficiency must be struck. Based on previous studies in the region [19,21], the 694 most relevant

energy bins, representing 95% of total resource and 87% of the time, were retained. This procedure, developed ad hoc for wave energy computations, has been shown to allow the transfer of high-resolution matrices considering practically 100% of the exploitable resource, given that 5% of the total resource that is disregarded corresponds to sea states under which WECs do not usually operate [21].

Each of the 694 deepwater energy bins selected constitutes a wave case, characterized by its spectral parameters (H_{mo}, T_e, θ_m) and considering a JONSWAP wave spectrum [28], which was successfully used in the North of Spain to define the energy distribution of sea states e.g. [30,31]. The JONSWAP spectrum can be obtained as [27]:

$$S(f) = \beta H_{1/3}^2 f_p^4 f^{-5} \exp\left[-1.25(f_p f^{-1})^4\right] \gamma^{\exp\left[-(f_p^{-1} f - 1)^2 / 2\zeta^2\right]} \tag{6}$$

$$\beta = \frac{0.0624}{0.23 + 0.0336\gamma - 0.185(1.9+\gamma)^{-1}} (1.094 - 0.01915 \ln \gamma) \tag{7}$$

$$\zeta = \begin{cases} 0.07, & f \le f_p. \\ 0.09, & f > f_p. \end{cases} \tag{8}$$

where β is the spectrum parameter, $H_{1/3}$ [m] is the significant wave height, f_p [Hz] is the peak wave frequency, ζ is width of the spectral peak region and γ is the peak enhancement factor, which is set to 3.3.

These conditions are used as boundary conditions of the spectral numerical SWAN (Simulation WAves Nershore), which computes the spectral evolution of the wave action density by solving the action balance equation [32]:

$$\frac{\partial N}{\partial t} + \frac{\partial (c_x N)}{\partial x} + \frac{\partial (c_y N)}{\partial y} + \frac{\partial (c_\omega N)}{\partial \omega} + \frac{\partial (c_\theta N)}{\partial \theta} = \frac{S}{\omega} \tag{9}$$

where N [m^2Hz^{-2}] is the wave action density, t [s], the time, c_x [ms^{-1}] and c_y [ms^{-1}] the propagation velocity in the geographic x- and y- space, c_θ [ms^{-1}] and c_ω [ms^{-1}] the propagation velocity in the θ- and ω-space, ω the relative frequency and S represent sources and sinks of the wave energy density due to different wave processes, such as generation, dissipation or non-linear wave-wave interactions.

In the present work, a high-resolution spatial grid is implemented whose characteristics were determined following previous studies in the region of interest e.g. [33]. The resolution of the grid cells is spatially varying, increasing from the open boundaries towards the sites of interest, thereby ensuring the appropriate computation of wave refraction and shoaling. The total number of cells of the computational grid is 35000, varying in size between 200 m at the study sites and 500 m at the offshore (ocean) boundaries (**Figure 7**).

[FIGURE 7]

In order to check the appropriateness of the grid size selected, the performance of four grids with different grid spacing, σ, (σ_1 = 350 m, σ_2 = 250 m, σ_3 = 200 m and σ_4 = 150) was determined. The increase in the performance of the different grid with increasing resolution is computed in terms of the variation of significant wave height, ΔH_{m0}, and wave power, ΔJ. For this purpose, the wave cases providing the largest amount of energy within each directional sector considered are propagated towards the coast, and the mean values of the aforementioned parameters, $\Delta H_{m0}^{\sigma_i-\sigma_{i+1}}$ and $\Delta J^{\sigma_i-\sigma_{i+1}}$, are computed (**Table 2**). It can be observed that the spectral results obtained are slightly

sensitive to an increase in the space resolution in the case of the grids with lower resolution, σ_1=350 and σ_2=250 m, with variations of the order of approx. 10^{-1} –10^{-2} m of H_{m0} and of 10^{0}–10^{-1} kW of J (σ_1-σ_2 and σ_2-σ_3). In contrast, there is no virtually modification between the spectral parameters values as computed by the grids with higher resolution (σ_3=200 m and σ_4=150m), with ballpark figures of ΔH_{m0} of the order of 10^{-3} –10^{-4} m and ΔJ of 10^{-1} –10^{-2} kW (σ_3-σ_4), overall one or two order lower than those provided by σ_1 and σ_2 grid spacing. On these bases, the appropriateness of the σ_2-grid (200 m of space resolution) is confirmed given that it provides similar numerical results as those computed by higher resolution grids (e.g. σ_1-grid) but with less computational effort. The numerical grid as interpolated with the bathymetry is shown in **Figure 8**.

[TABLE 2]

[FIGURE 8]

The resulting wave data consist of the main wave parameters H_{m0}, T_e, θ_m for each wave case propagated at each selected location. Furthermore, the power per meter of wave front, J, is now computed by considering the complete spectrum of each resulting wave case at the three different locations as:

$$J = \rho g \int_0^{2\pi} \int_0^{\infty} S(f,\theta) c_g(f,d) df d\theta \qquad (10)$$

where c_g [ms^{-1}] is the wave group celerity.

2.4.2. Resource at the locations of interest

The next step consists in characterizing the available energy at the three sites of interest in the form of high-resolution characterization matrices. The characterization matrix at each location is reconstructed by following the same steps as in the case of the deepwater buoy, the only difference being that the θ_m discretization is not taken into account given that the currently available WECs power matrices do not provide directional information. As a result, a two-dimensional matrix (H_{m0}, T_e) is obtained at each location A, B and C (**Figure 9**).

[FIGURE 9]

The total annual available energy per meter of wave front, $E_{W,T}$ [Whm^{-1}], is therefore given by:

$$E_{W,T} = \sum_{i=1}^{n} E_{b,i} \tag{11}$$

where $E_{b,i}$ represents the energy provided by each energy bin at the coastal locations and n the total number of the resulting bins. The total energy available reaches values up to 110 MWhm^{-1} at point A, 149 MWhm^{-1} at point B, and 186 MWhm^{-1} at point C, i.e. values of 12.5 kWm^{-1}, 17 kWm^{-1}, 21 kWm^{-1}at points A, B and C, respectively, in terms of average annual power.

2.4.3. Parametric estimation of power performance

The final step of the procedure consists in the computation of the performance of the selected WECs at the sites of interest. First, the total energy production of a specific WEC at a given location, $E_{WEC,T}$ [Wh], is obtained by combining the power matrix of

the WEC with the characterization matrices computed at the sites of interest. This involves combining each value of power output, P_i [W], from the WEC power matrix, with its corresponding value of occurrence, $O_{b,i}$ [h], in the characterization matrices. The total energy production is thus obtained as:

$$E_{WEC,T} = \sum_{i=1}^{n} P_i O_{b,i} \tag{12}$$

where n is the number of energy bins, which depends on the level of resolution of the matrices (size of energy bins) to be combined (the resolution of the power matrix and the characterization matrix should be of the same level for accurate power production estimations).

The total annual energy produced largely depends on the rated power, P_r [W], of the WEC considered; consequently, the energy production obtained, for all its interest, does not provide the full picture of the WEC performance. Therefore, in order to obtain reliable comparisons among the various technologies at the sites considered, the capacity factor, C_f [%] is also computed, defined as the ratio between the total energy production of a WEC over a certain period, $E_{WEC,T}$, and the total energy that it would have produced over the same period, had it operated at its rated power ($P_r h$):

$$C_f = \frac{E_{WEC,T}}{P_r h} 100 \tag{13}$$

where h is the total number of hours over a given period (a year in the present case).

3. Results and discussion

3.1. Wave energy resource at the sites of interest

The wave energy distribution presents significant differences among the study sites (**Figure 9**) even though they are not far away. In the case of Point C, the site with the greatest water depth, the bulk of the energy is provided by wave heights in the range 2 – 6 m and energy periods in the range 8 – 12 s, with the most energetic bins (the brownish hues of the colour scale) supplying up to 6 $MWhm^{-1}$ of the total energy. In the case of point B, the resource distribution is clearly different, being more concentrated within certain ranges: 1.5 – 4 m of H_{m0}, and 7 – 11 s of T_e, with the most energetic bins attaining no more than 5 $MWhm^{-1}$. Finally, the concentration of the energy resource is even more evident at Point A. At this location, the wave energy is mainly supplied by energy bins with 1.5 – 3 m of H_{m0} and 6 – 9.5 s of T_e, providing up to 3.5 $MWhm^{-1}$. All in all, as the water depth reduces wave energy progressively concentrates in a narrower band of wave height and period, with the energy bins corresponding to sea states with less wave power providing the lion's share of the total energy thanks to their greater occurrence. In other words, as the wave field approaches the shoreline, the wave resource tends to concentrate within intervals of reduced wave height and, to a lesser extent, wave period; these differences with respect to the offshore (deepwater) wave resource must be taken into account in determining the performance of the WECs at the study sites.

3.2. Energy performance of WEC-site combinations

The results of the annual energy production per device unit, $E_{WEC,T}$, are shown in **Figure 10**. The device generating the largest amount of energy is B-OF at Point A with 2656.05 MWh, closely followed by AWS at Point C with 2406.99 MWh. Regarding Point B, the total energy that can be generated is substantially less, with a maximum of 1657.26 MWh with F-OWC. It is interesting to note that a greater energy output is attained at

Point C than at Point B, even though the resource available is greater at Point B, thanks to the overall larger values of power output of the B-OF device, as expressed by its power matrix (**Figure 4**).

[FIGURE 10]

In order to determine more accurately the performance of the different WEC-site combinations, the capacity factor is also computed by means of Eq. (10), and the results are shown in **Figure 11**. This ratio is equivalent to the Full Load Hours, *FLH*, also known as Equivalent Hours, E_h, commonly used in wind energy studies, and it is fundamental in assessing the suitability of a WEC for a specific site.

In contrast to the energy production figures, the devices providing the highest values of C_f are Bref-HB, reaching 15.96 % and 18.69 % at Points A (36 m of water depth) and B (68 m), respectively, and Pelamis, with 18.48 % and 21.18 % at points B (68 m) and C (113 m), respectively. It is important to note that the higher values of the capacity factor obtained by the same technologies at larger water depths—e.g. Bref-HB and Pelamis, as previously mentioned, or F-OWC which increases from 6.57 % (at a 69 m water depth) to 8.19 % (at a 113 m water depth)—results from the complex distribution of the wave energy resource across wave heights and periods. In effect, at Point C (113 m) the energy bins supplying the bulk of the energy are spread over a wide range of conditions, including high power conditions with larger occurrence than at points A and B within which the aforementioned devices provide high efficiency (power output).

4. Conclusions

In installing a wave energy operation, the selection of the technology and location should be carried out on the basis of a thorough knowledge of all the relevant factors affecting its exploitation. For this purpose, the performance of different WECs should be accurately computed at the locations of interest. In this work, the area near the Port of Burela (Galicia, NW Spain) was used as a case study to illustrate a comprehensive procedure to accurately compute the performance of different WECs, at locations not representing potential interferences with other uses of the marine space.

The first step consists in determining the areas of interest, avoiding environmental impacts and socioeconomic interferences on e.g. fishing and aquaculture, maritime routes and marine reserves. On the basis of this information, three sites are selected: Points A, B and C, in water depths of 36 m, 69 m and 113 m, respectively. At these locations of virtually the totality of the exploitable resource is characterized by means of a nonconventional methodology based on the propagation of a large number intervals of wave height, energy period and wave direction (energy bins) obtained from deepwater buoy records. The procedure is implemented with high-resolution intervals (0.5 m of H_{m0}, 0.5 s of T_e and 22.5º of θ_m).

The annual average power figures obtained are 12.5 kW m^{-1}, 17.0 kW m^{-1} and 21.0 kW m^{-1} at points A, B and C, respectively. This means that there exist variations of up to 25% in sites at very short distances from one another, which underlines the need for implementing numerical models of high-spatial resolution—an aspect usually disregarded in the conventional approach. In addition, it is clear from the computed characterization matrices that these differences concern not only the total available energy but also their distribution across wave heights and periods, with a tendency for energy concentration within specific intervals depending on the characteristics of the coastal site of interest. This tendency, which is the result of the refraction and shoaling

of waves in their propagation towards the coast, has been shown to affect significantly the performance of WECs.

By combining each resource characterization matrix with the power matrix of the WECs of interest, the total energy production and performance of a given WEC-site combination were determined. It was found that the device providing the largest energy production is B-OF at Point A, with an annual output of 2656.05 MWh, followed by AWS at Point C with 2406.99 MWh. Given that the water depth is much greater at Point C than at Point A, these results indicate that, although the wave climate is generally more energetic at deeper sites, this does not lead necessarily to a greater energy output.

Another element to be considered in analyzing the performance and suitability of the WEC-site combinations considered is the capacity factor. It was found that, with the exception of F-OWC, the devices considered attain values of the capacity factor in the range of 15 – 21%, which can be considered as adequate for commercial exploitation. In particular, the largest value is obtained by Pelamis at a water depth of 113 m (Point C), with C_f = 21.18 %. This result is of particular interest given that the energy production obtained by this WEC-site combination (1391.59 MWh/year) is about half of that with the greatest energy production. This underlines the importance of considering high-resolution distribution of the resource amongst energy bins (at least with the same level of resolution as that provided by the WECs' power matrices) for accurate energy production and performance computations.

In sum, the present work shows the importance of considering an integrated approach in defining the most appropriate WEC and location for installing a wave farm in a region. In particular, the procedure implemented allows the determination of the WEC providing the largest performance at various locations where the environmental impacts

and the potential negative socioeconomic effects are virtually non-existent, or in other words, leading to an effective integrated coastal zone management when introducing a new coastal use, as it is the case of an operation of a wave farm.

Acknowledgements

This work was conducted within the framework of the project *Online Application and High Resolution Management System for the Exploitation of the Wave Energy Resource in the Atlantic Region of Europe* supported by the Iberdrola Foundation. During this work Néstor Areán has been supported by Xunta de Galicia (Programa de Apoyo a la Etapa Predoctoral en las Universidades del SUG). Gregorio Iglesias wishes to acknowledge the support obtained from the European Commission through a Marie Curie fellowship (PCIG13-GA-2013-618556, WAVEIMPACT). The authors are grateful to State Ports for the wave buoy data.

List of symbols

H_{m0} spectral significant wave height [m]

T_e energy period [s]

m_n n-th spectral moment [m^2Hz^{-n}]

f wave frequency [Hz]

S spectral density [$m^2Hz^{-1}deg^{-1}$]

θ wave direction [º]

θ_m mean wave direction [º]

O_b occurrence of an energy bin [h]

E_b energy provided by each energy bin [Whm^{-1}]

J wave power per unit width computed using linear theory [kWm^{-1}]

ρ seawater density [kgm^{-3}]

g gravitational acceleration [ms^{-2}]

k wave number [m^{-1}]

d local water depth [m]

β spectrum parameter [-]

$H_{1/3}$ significant wave height [m]

f_p peak wave frequency [Hz]

ζ width of spectral peak region [-]

γ peak enhancement factor [-]

N wave action density [m^2Hz^{-2}]

t time [s]

c_x propagation velocity in the x-space [ms^{-1}]

c_y propagation velocity in the y-space [ms^{-1}]

c_θ propagation velocity in the θ-space [ms^{-1}]

c_ω propagation velocity in the ω-space [ms^{-1}]

ω relative frequency [Hz]

c_g group velocity [ms^{-1}]

$E_{W,T}$ total available energy per meter of wave front [Whm^{-1}]

n number of bins [bins]

$E_{WEC,T}$ total energy production of a WEC [Wh]

P power output [W]

P_r rated power [W]

C_f capacity factor [%]

h number of hours [h]

FLH Full Load Hours [h]

Eh Equivalent Hours [h]

References

[1] Guedes Soares C, Rute Bento A, Gonçalves M, Silva D, Martinho P. Numerical evaluation of the wave energy resource along the Atlantic European coast. Computers & Geosciences 2014;71:37-49.

[2] Rusu L, Onea F. Assessment of the performances of various wave energy converters along the European continental coasts. Energy 2015;82:889-904.

[3] Kalogeri C, Galanis G, Spyrou C, Diamantis D, Baladima F, Koukoula M et al. Assessing the European offshore wind and wave energy resource for combined exploitation. Renewable Energy 2017;101:244-64.

[4] Mustapa MA, Yaakob OB, Ahmed YM, Rheem C, Koh KK, Adnan FA. Wave energy device and breakwater integration: A review. Renewable and Sustainable Energy Reviews 2017;77:43-58.

[5] Iglesias G, López M, Carballo R, Castro A, Fraguela JA, Frigaard P. Wave energy potential in Galicia (NW Spain). Renewable Energy 2009;34:2323-33.

[6] Babarit A, Hals J, Muliawan MJ, Kurniawan A, Moan T, Krokstad J. Numerical benchmarking study of a selection of wave energy converters. Renewable Energy 2012;41:44-63.

[7] Fadaeenejad M, Shamsipour R, Rokni SD, Gomes C. New approaches in harnessing wave energy: With special attention to small islands. Renewable and Sustainable Energy Reviews 2014;29:345-54.

[8] Al-Habaibeh A, Su D, McCague J, Knight A. An innovative approach for energy generation from waves. Energy Conversion and Management 2010;51:1664-8.

[9] Fernandez H, Iglesias G, Carballo R, Castro A, Fraguela JA, Taveira-Pinto F et al. The new wave energy converter WaveCat: Concept and laboratory tests. Mar Struct 2012;29:58-70.

[10] López I, Pereiras B, Castro F, Iglesias G. Holistic performance analysis and turbine-induced damping for an OWC wave energy converter. Renewable Energy 2016;85:1155-63.

[11] Iglesias G, Carballo R. Wave resource in El Hierro—an island towards energy self-sufficiency. Renewable Energy 2011;36:689-98.

[12] Sierra JP, González-Marco D, Sospedra J, Gironella X, Mösso C, Sánchez-Arcilla A. Wave energy resource assessment in Lanzarote (Spain). Renewable Energy 2013;55:480-9.

[13] Rusu E, Onea F. Estimation of the wave energy conversion efficiency in the Atlantic Ocean close to the European islands. Renewable Energy 2016;85:687-703.

[14] Carballo R, Sánchez M, Ramos V, Fraguela JA, Iglesias G. The intra-annual variability in the performance of wave energy converters: A comparative study in N Galicia (Spain). Energy 2015;82:138-46.

[15] Astariz S, Iglesias G. The collocation feasibility index – A method for selecting sites for co-located wave and wind farms. Renewable Energy 2017;103:811-24.

[16] Ghosh S, Chakraborty T, Saha S, Majumder M, Pal M. Development of the location suitability index for wave energy production by ANN and MCDM techniques. Renewable and Sustainable Energy Reviews 2016;59:1017-28.

[17] Vasileiou M, Loukogeorgaki E, Vagiona DG. GIS-based multi-criteria decision analysis for site selection of hybrid offshore wind and wave energy systems in Greece. Renewable and Sustainable Energy Reviews 2017;73:745-57.

[18] Arean N. A comprehensive decision-making tool for wave energy exploitation: A case study in the North coast of Galicia. 2016.

[19] Carballo R, Sánchez M, Ramos V, Castro A. A tool for combined WEC-site selection throughout a coastal region: Rias Baixas, NW Spain. Applied Energy 2014;135:11-9.

[20] Iglesias G, Carballo R. Choosing the site for the first wave farm in a region: A case study in the Galician Southwest (Spain). Energy 2011;36:5525-31.

[21] Carballo R, Sánchez M, Ramos V, Taveira-Pinto F, Iglesias G. A high resolution geospatial database for a wave energy exploitation. Energy 2014;68:572-83.

[22] Veigas M, López M, Iglesias G. Assessing the optimal location for a shoreline wave energy converter. Applied Energy 2014;132:404-11.

[23] Carballo R, Sánchez M, Ramos V, Fraguela JA, Iglesias G. Intra-annual wave resource characterization for energy exploitation: A new decision-aid tool. Energy Conversion and Management 2015;93:1-8.

[24] Carballo R, Iglesias G. A methodology to determine the power performance of wave energy converters at a particular coastal location. Energy Conversion and Management 2012;61:8-18.

[25] A. Alexander K, A. Wilding T, Jacomina Heymans J. Attitudes of Scottish fishers towards manire renewable energy. Marine Policy 2013;37:239-44.

[26] Zanuttigh B, Angelelli E, Kortenhaus A, Koca K, Krontira Y, Koundouri P. A methodology for multi-criteria design of multi-use offshore platforms for marine renewable energy harvesting. Renewable Energy 2016;85:1271-89.

[27] Goda Y. Random seas and design of maritime structures. Singapore: World Scientific, 2000.

[28] Hasselmann DE. Directional wave spectra observed during JONSWAP 1973. J Phys Oceanogr 1980;10:1264-80.

[29] Dean RG, Dalrymple RA. Water Wave Mechanics for Engineers and Scientists. : World Scientific, 1991.

[30] Vidal Pascual C. Análisis de la energía del oleaje en las costas españolas. Revista de Obras Públicas 1986;133:95-108.

[31] López M, Veigas M, Iglesias G. On the wave energy resource of Peru. Energy Conversion and Management 2015;90:34-40.

[32] Booij N, Ris RC, Holthuijsen LH. A third-generation wave model for coastal regions 1. Model description and validation. Journal of Geophysical Research C: Oceans 1999;104:7649-66.

[33] Silva D, Bento AR, Martinho P, Guedes Soares C. High resolution local wave energy modelling in the Iberian Peninsula. Energy 2015;91:1099-112.

Figure Captions

Figure 1. Location of the study area on the Galician coast, NW Spain.

Figure 2. Spatial distribution of the marine uses and environmental areas of interest nearby Port of Burela (NW Spain).

Figure 3. Location of the selected Points (A, B and C) for installing a wave farm.

Figure 4. Power matrices expressed in terms of power output (kW) for the different wave conditions (intervals of significant wave height, H_{m0}, and energy period, T_e) of the devices selected e.g. [6]: a) F-OWC, Floating Oscilating Water Column ; b) B-OF, Bottom-fixed Oscillating Flap; c) B-HBA, Bottom-fixed heave-Buoy Array; d) Pelamis; e) Bref-HB, Small bottom-referenced Heaving Buoy; and f) AWS, Archimedes Wave Swing.

Figure 5. Annual wave rose based on deepwater wave buoy data.

Figure 6. Deepwater characterization matrix. [The numbers represent the occurrence expressed in hours in an average year; the isolines, the wave power; and the colour scale, the total energy provided by each energy bin in an average year.]

Figure 7. Location of the deepwater buoy and the selected sites within the numerical grid. For clarity, only one in four coordinate lines is shown.

Figure 8. Bathymetry of the study area as interpolated into the computational grid.

Figure 9. Characterization matrices of the wave resource at points A, B and C. [The numbers represent the occurrence expressed in hours in an average year; the isolines, the wave power; and the colour scale, the total energy provided by each energy bin in an average year.]

Figure 10. Energy production (MWh/year) for the different WEC-site combinations considered.

Figure 11. Capacity factor (%) for the different WEC-site combinations considered.

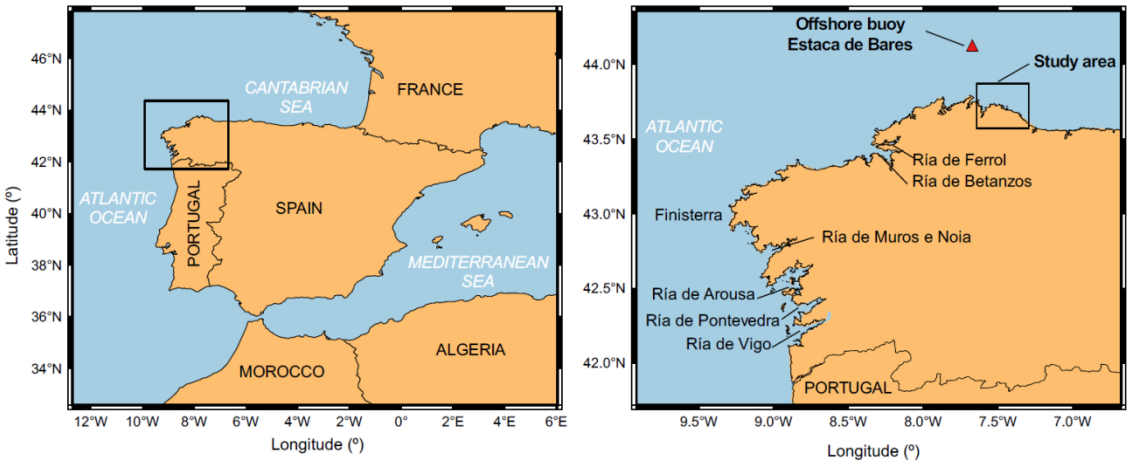

Figure 1. Location of the study area on the Galician coast, NW Spain.

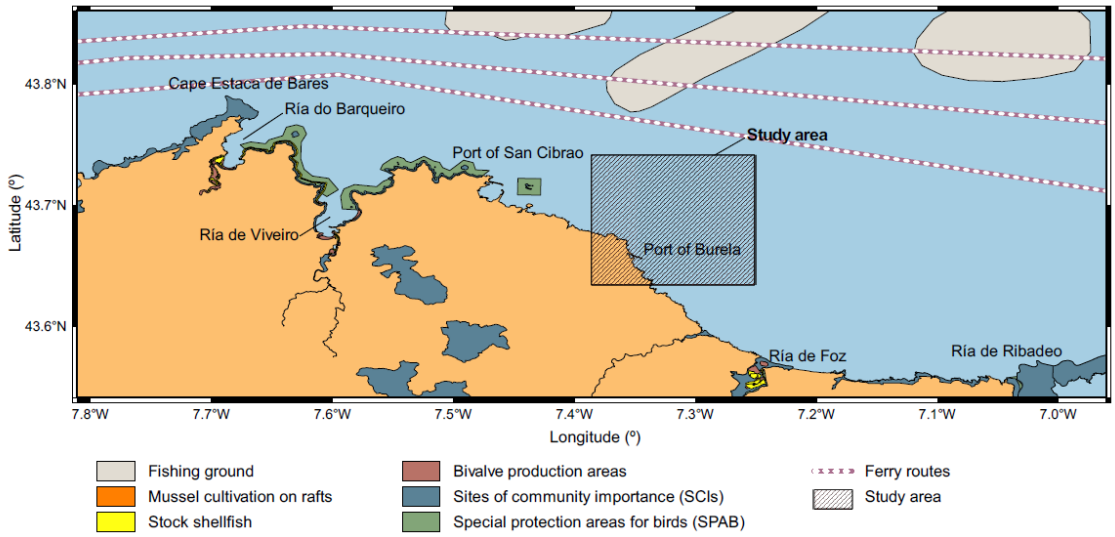

Figure 2. Spatial distribution of the marine uses and environmental areas of interest nearby Port of Burela (NW Spain).

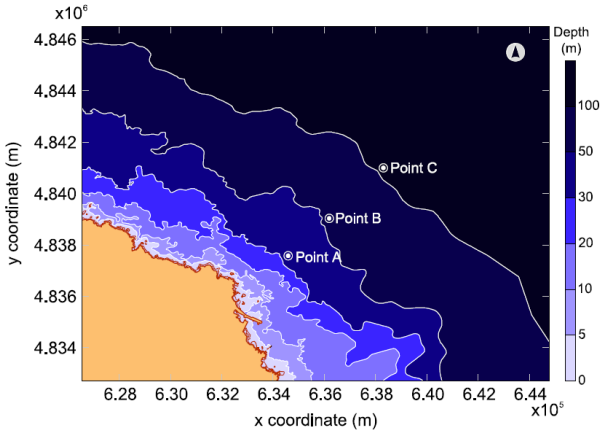

Figure 3. Location of the selected Points (A, B and C) for installing a wave farm.

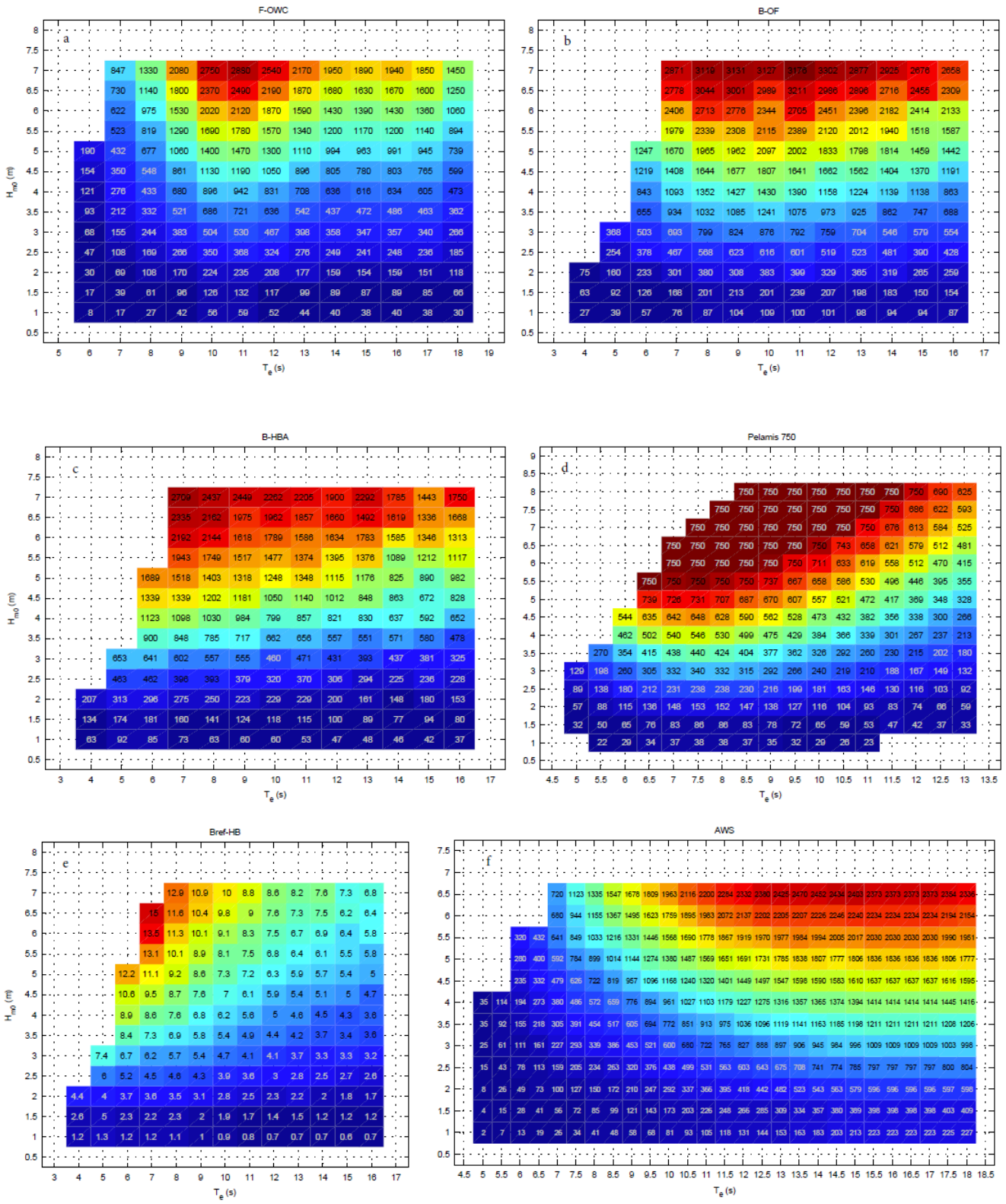

Fig. 4. Power matrices in terms of power output (kW) for the different wave conditions (intervals of significant wave height, H_{mo}, and energy period, T_e) of the devices selected e.g. [6]: a) F-OWC, Floating Oscilating Water Column ; b) B-OF, Bottom-fixed Oscillating Flap; c) B-HBA, Bottom-fixed heave-Buoy Array; d) Pelamis; e) Bref-HB, Small bottom-referenced Heaving Buoy; and f) AWS, Archimedes Wave Swing.

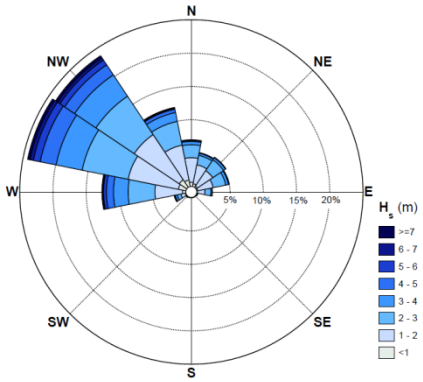

Figure 4. Annual wave rose based on deepwater wave buoy data.

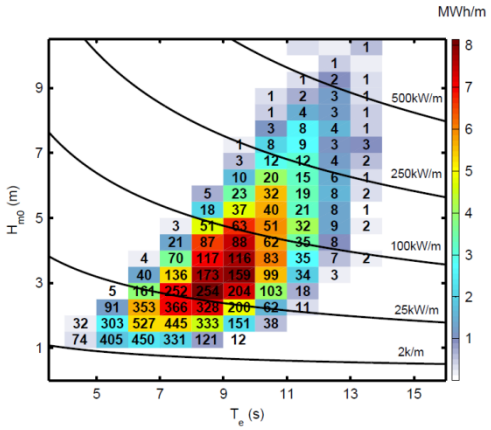

Figure 6. Deepwater characterization matrix. [The numbers represent the occurrence expressed in hours in an average year; the isolines, the wave power; and the colour scale, the total energy provided by each energy bin in an average year.]. (For interpretation of the references to colour in this figure legend, the reader is referred to the web version of this article.)

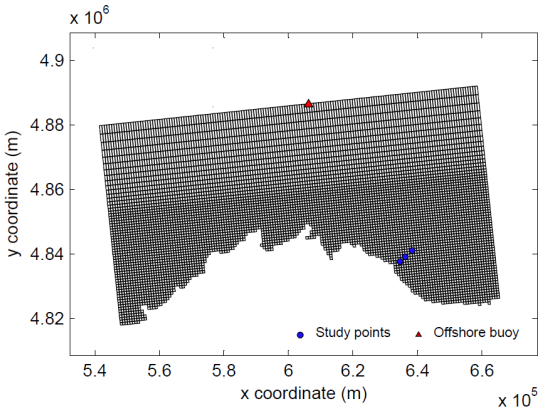

Figure 7. Location of the offshore buoy and the selected sites within the numerical grid. For clarity, only one in four coordinates is shown.

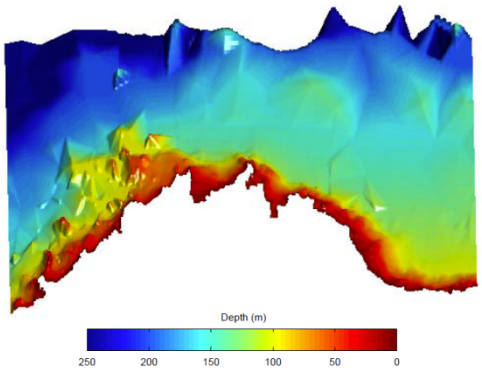

Figure 8. Bathymetry of the study area as interpolated into the computational grid.

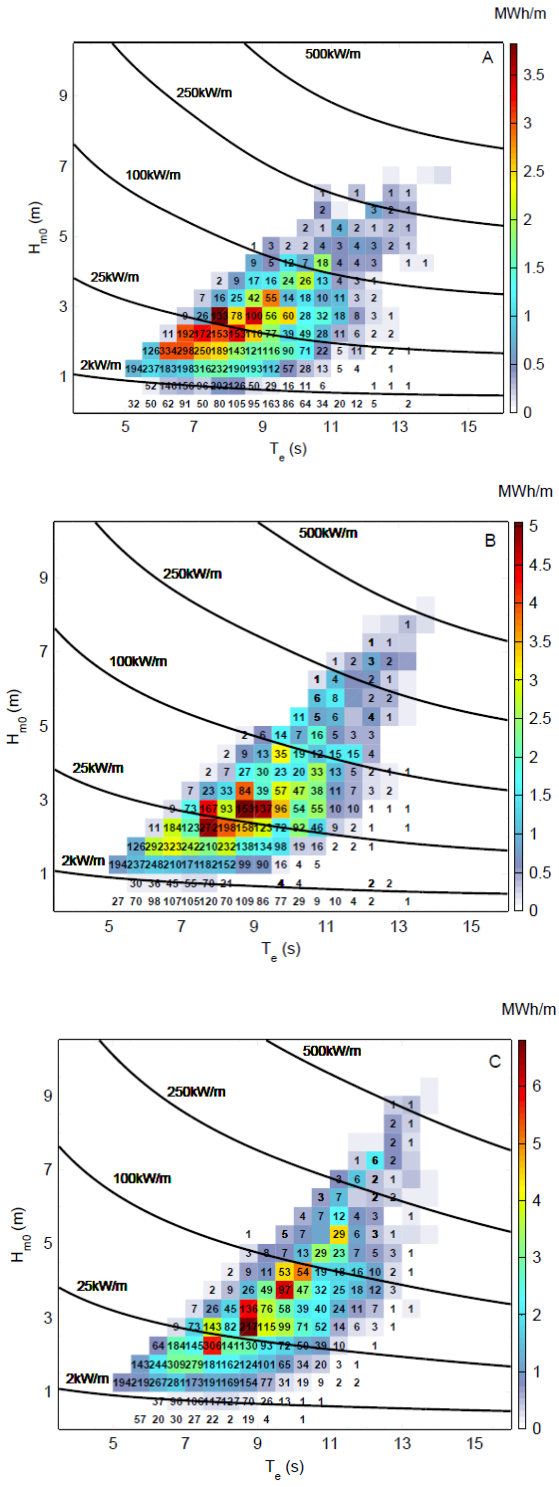

Figure 9.Characterization matrices of the wave resource at points A, B and C. [The numbers represent the occurrence expressed in hours in an average year; the isolines, the wave power; and the colour scale, the total energy provided by each energy bin in an average year.]. (For interpretation of the references to colour in this figure legend, the reader is referred to the web version of this article.)

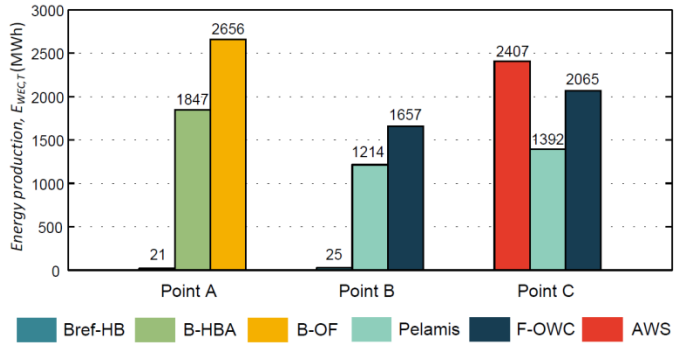

Figure 10. Energy production (MWh/year) for the different WEC-site combinations considered.

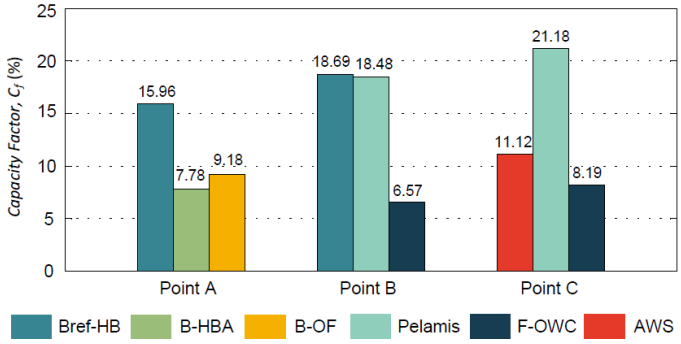

Figure 11. Capacity factor (%) for the different WEC-site combinations considered.

Table 1. Characteristics of WEC-site combinations considered

Location	Depth (m)	WEC	Power matrix resolution		P_r (kW)
			H_{m0} (m)	T_e (s)	
A	36.48	Bref-HB	0.5	1	15
		B-HBA	0.5	1	2709
		B-OF	0.5	1	3302
B	68.54	Bref-HB	0.5	1	15
		Pelamis	0.5	0.5	750
		F-OWC	0.5	1	2880
C	112.8	AWS	0.5	0.5	11.12
		Pelamis	0.5	0.5	750
		F-OWC	1	1	2880

Table 2. Variations of H_{m0}, ΔH_{m0} (m), and variations of J, ΔJ (kW), as computed by different numerical grids (σ_1, σ_2, σ_3, σ_4) for the most energetic case of each directional sector considered (Cases 1-9).

Nº Case	Θ (º)	H_{m0} (m), T_e (s)	$\Delta H_{m0}^{\sigma_1-\sigma_2}$	$\Delta J^{\sigma_1-\sigma_2}$	$\Delta H_{m0}^{\sigma_2-\sigma_3}$	$\Delta J^{\sigma_2-\sigma_3}$	$\Delta H_{m0}^{\sigma_3-\sigma_4}$	$\Delta J^{\sigma_3-\sigma_4}$
1	270	4.26, 9.25	6.69×10^{-2}	1.52	2.47×10^{-2}	6.93×10^{-1}	4.05×10^{-4}	1.37×10^{-1}
2	292.5	4.26, 9.75	9.18×10^{-2}	2.27	5.43×10^{-2}	1.53	1.20×10^{-2}	2.23×10^{-1}
3	315	3.77, 9.75	7.11×10^{-2}	1.73	4.20×10^{-2}	1.3045	4.18×10^{-4}	2.54×10^{-1}
4	337.5	2.28, 8.25	3.66×10^{-2}	4.33×10^{-1}	1.91×10^{-2}	3.17×10^{-1}	2.20×10^{-3}	4.06×10^{-2}
5	0	2.77, 8.25	3.38×10^{-2}	5.42×10^{-1}	2.31×10^{-2}	4.63×10^{-1}	4.50×10^{-3}	1.34×10^{-1}
6	22.5	2.28, 6.75	3.03×10^{-2}	2.82×10^{-1}	2.12×10^{-2}	2.60×10^{-1}	4.15×10^{-4}	5.12×10^{-2}
7	45	2.28, 6.25	3.20×10^{-2}	2.70×10^{-1}	2.50×10^{-2}	2.68×10^{-1}	1.50×10^{-3}	4.01×10^{-2}
8	67.5	2.28, 5.75	3.40×10^{-2}	3.01×10^{-1}	3.02×10^{-2}	3.07×10^{-1}	4.70×10^{-3}	9.97×10^{-2}
9	90	2.28, 5.75	4.18×10^{-2}	3.15×10^{-1}	1.57×10^{-2}	1.63×10^{-1}	3.60×10^{-4}	7.30×10^{-3}